No. 68-87
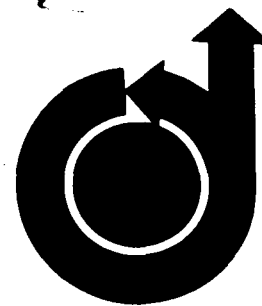
ANALYSIS OF MPD ARCS WITH NONEQUILIBRIUM IONIZATION

by

R. K. SEALS JR. and H. A. HASSAN
North Carolina State University
Raleigh, North Carolina

AIAA Paper
No. 68-87

GPO PRICE $ _____

CFSTI PRICE(S) $ _____

Hard copy (HC) ___3.00___

Microfiche (MF) ___,65___

ff 653 July 65

AIAA 6th Aerospace Sciences Meeting

NEW YORK, NEW YORK/JANUARY 22-24, 1968

ANALYSIS OF MPD ARCS WITH NONEQUILIBRIUM IONIZATION*

R. K. Seals, Jr., and H. A. Hassan
North Carolina State University
Raleigh, North Carolina

Abstract

A quasi one-dimensional analysis of the MPD arc which takes into consideration finite rate processes and allows for a variable area is presented. Starting from low subsonic velocities at the entrance, the governing equations are integrated through the transonic region into the supersonic region for an argon propellant at low mass flow rates. The results show that the electron temperature is well predicted by the theory; however, calculated velocities are roughly half the measured values. The current densities peak in the neighborhood of the cathode tip and they do not exhibit any unusual features in the transonic region. Comparison of calculated and measured power inputs led to the conclusion that most of the published data are taken in situations where transition to supersonic velocities takes place outside the engine; in such situations, the possibility of gas entrainment exists and the effective and metered mass flow rates are not necessarily equal.

1. Introduction

In a recent review article, Nerheim and Kelly[1] stressed the limited progress that was made in understanding the thrust mechanism and in defining the proper test environment for MPD arcs. This situation is due mainly to the lack of uniform and detailed diagnostic measurements, especially within the engine itself, and to the complexity of the analytical problem.

Because most of the uncertainties seem to be associated with low mass flow devices, the calculations presented here, which are based on a quasi one-dimensional model, are carried out for low mass flow rates. The governing equations are the conservation equations of mass, momentum, and energy of the various plasma constituents[2]; thus, the analysis takes into consideration an electron temperature different from the gas temperature, ion slip, finite ionization rates, and heat loss. The geometry and magnetic field distribution are those of Ref. 3 which are typical of existing devices.

In the MPD arc, the propellant enters at low subsonic velocities and somewhere within or outside the device the Mach number becomes supersonic. Thus any realistic model must cope with the problem of carrying the integration through the sonic singularity. Since the sonic point is a saddle point, numerical integration through such a point is very complicated, especially when the electron temperature is different from the gas temperature.

The complexity of the analytical model is due, in part, to the nature of the sonic singularity. In this work a method has been found whereby one can remove such a singularity. This is achieved by utilizing the momentum and energy fluxes, instead of the velocity and temperature, as the dependent variables.

The magnetic field distribution given in Ref. 3 is limited to a range of about two anode diameters downstream of the exit plane. Because of this, the calculations presented here were terminated at approximately the same distance. Comparison with the measurements of Ref. 3 shows that the calculated electron temperature agrees well with experiment; however, the velocities are underestimated by a factor of about 2.

2. Formulation of the Problem

A. Qualitative Formulation

Since a one-dimensional model is employed to analyze the flow in the geometry shown in Fig. 1, it would be desirable, as a first step, to recall some of the pertinent results of the one-dimensional compressible flow theory[4] in the variable area ducts. The first concerns flow with heat addition; when heat is added to a flow in a variable area duct, the sonic velocity occurs somewhere in the divergent section. This means that in the MPD arc, where power is being added at the rate of $\vec{j} \cdot \vec{E}$ per unit volume, the assumption that the sonic velocity occurs at the throat is not valid.[5] Also, heating accelerates a subsonic flow and decelerates a supersonic flow.

The second result concerns the interpretation of the experimental data; if the exit velocity is sonic or supersonic, a disturbance outside the duct cannot influence the flow within the duct. The above result implies that, if the tank pressure is below a certain critical value which results in a sonic or supersonic exit, the thrust should be independent of the test environment. If, on the other hand, the thrust varies with the tank pressure, then this would imply that the exit Mach number is subsonic.

In this work, the motion of the various species is referred to the center of mass; thus the Mach number and sonic velocity refer to the mean motion. For smooth transition from subsonic to supersonic, the combined influence of the $\vec{j} \times \vec{B}$ force and area change must outweigh the net power input

into the arc. Using representative values of power inputs and magnetic field strengths and typical geometries one finds that, in the absence of losses, the influence of the power density far outweighs that of area change and body force. Thus, one is tempted to conclude that the maximum Mach number within the engine is unity. This, however, may not be the case because wall losses and the fact that not all the power is added within the engine may be such that a transition to supersonic velocities can take place within the engine.

Because it is not possible to infer the location of the sonic point from available experimental data, a variety of models for the MPD arcs are explored here. Thus, for a given geometry, magnetic field distribution, mass flow rate, and total current, the first model assumes that power addition takes place within the engine only. Outside the engine, it is assumed that the plasma is magnetically contained. A wide range of entrance conditions was investigated and it was found that, in the absence of losses (other than radiation), the calculated power density was such that the maximum Mach number attained within the electrode region was unity. A calculation of the total power input showed that it was a small fraction of the experimentally reported values and this resulted in axial velocities much below those measured experimentally. Thus, it was concluded that such a model cannot approximate the behavior of typical MPD arcs.

Experimental and theoretical evidence suggests that in most cases large currents and potential gradients exist in the plume and that losses represent a significant fraction of the power input. Thus, a representative one-dimensional model should allow for the existence of a virtual anode extending downstream of the engine, and power losses. The shape and extent of such a virtual anode and the magnitude of the power loss cannot, however, be determined from one-dimensional considerations and some assumptions must be introduced.

The second model employed here assumes that outside the electrode region the plasma is magnetically contained and the virtual anode coincides with the magnetic nozzle. It should be noted that, within the framework of one-dimensional theory, such an assumption does not predetermine the acceleration mechanism. To specify the extent of the virtual anode, one needs to specify the power input; the virtual anode extends to the point where the computed power input equals the specified power input. Beyond this point, it is assumed that no energy is added to the plasma. The power loss in the supersonic region was chosen in such a way as to ensure an increasing Mach number. In the subsonic region, the power loss was assumed to be some fraction of the total power.
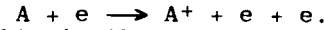
B. Analytical Formulation

The analysis is based on the conservation equations of a singly ionized monatomic gas.[2] For steady flow, the species continuity equation can be written as

$$\nabla \cdot (n_s \vec{v}_s) = \nabla \cdot [n_s(\vec{v} + \vec{V}_s)] = R_s \qquad (1)$$

where n_s, $\vec{v}_s$, $\vec{V}_s$, and R_s are number density, mean and diffusion velocity, and production rate in particles/volume of species s, respectively, while $\vec{v}$ is the mean velocity of the entire mixture. The over-all continuity equation is obtained by multiplying Eq. (1) by m_s, and summing,

$$\nabla \cdot (\rho \vec{v}) = 0, \quad \rho = \Sigma \rho_s, \quad \rho_s = n_s m_s \qquad (2)$$

where m_s is the particle mass of species s. For the plasma under consideration, the dominant ionization reaction is
$$A + e \longrightarrow A^+ + e + e.$$
Opposing this is the recombination reaction,
$$A^+ + e + e \longrightarrow A + e,$$
where A denotes an atom, A^+ an ion, and e an electron. Based on these reactions,

$$R_e = R_i = -R_a = \left(n_e n_a - \frac{n_i n_e^2}{K}\right) f(T_e) \qquad (3)$$

where

$$K = 2 \frac{g_i}{g_a} \left(\frac{2\pi m_e k T_e}{h^2}\right)^{3/2} \exp(-I/kT_e) \qquad (4)$$

and

$$f(T_e) = \frac{(8/\pi m_e k T_e)^{1/2}}{kT_e} \int_I^\infty$$
$$\times \exp(-\xi/kT_e) Q(\xi) \xi d\xi \qquad (5)$$

where g_i, g_a are the degeneracies of the ground states of the ions and atoms, k, the Boltzmann constant; h, Planck's constant; I, the first ionization potential; T_e, the electron temperature; and Q is the ionization cross section.

In a one-dimensional analysis, where wall effects are neglected, the contribution to the number flux from diffusion, $n_s \vec{V}_s$, is usually neglected. When the resulting equation is combined with Eq. (2), one obtains

$$n\vec{v} \cdot \nabla \alpha = R_i, \quad n = \Sigma n_s \qquad (6)$$

where α is the degree of ionization defined by

$$n_e = n_i = \alpha, \quad n_a = (1-\alpha)n \qquad (7)$$

and n is the number density of the nuclei.

The momentum equations give, in addition to the mean velocities, the ion and electron current densities. If the viscous stresses are neglected, the over-all momentum equation can be expressed as

$$\rho \frac{D\vec{v}}{dt} + \nabla P = \vec{j} \times \vec{B}, \quad P = \Sigma P_s = \Sigma k n_s T_s \qquad (8)$$

where P, $\vec{j}$, and $\vec{B}$ denote, respectively, the pressure, current density, and magnetic field strength. The expressions derived by Cowling[7] for the ion current density and the

total current density are employed here. Assuming that collision cross sections of charged particles are much larger than cross sections of collisions involving neutral atoms the current densities can be written as

$$\vec{j} = \frac{\sigma_0}{\omega_e \tau_{ie}(1+\lambda^2)} \left\{ \lambda[\vec{E}^* - \frac{\vec{E}\cdot\vec{B}}{B}\vec{B}] - \frac{\vec{E}^* \times \vec{B}}{B} \right\}$$
$$+ \sigma_0 \left(\frac{\vec{E}\cdot\vec{B}}{B^2}\right)\vec{B}$$

and

$$\vec{j}_i = [\lambda - (\omega_e\tau_{ie})^{-1}]\frac{\vec{j}\times\vec{B}}{B} \qquad (9)$$

with

$$\vec{j} = \vec{j}_e + \vec{j}_i$$
$$\lambda = (\omega_e\tau_{ie})^{-1} + 2(1-\alpha)^2\omega_i\tau_{ia}$$

$$\vec{E}^* = \vec{E} + \vec{v}\times\vec{B}, \quad \sigma_0 = n_e e^2\tau_{ie}/m_e, \quad \omega_s = eB/m_s$$

$$Z_{st} = (3/2n_s Z_{st})\left[2k\left(\frac{T_s}{m_s} + \frac{T_t}{m_t}\right)\right]^{-1/2} \qquad (10)$$

where $\vec{E}$ and Z_{st} denote the electric field and diffusion cross section, respectively.

Three energy equations are needed to determine the electron, ion, and neutral temperatures. However, since the mass of the atom is almost equal to the mass of the ion, the assumption is usually made that the ion and neutral temperatures are equal. Thus, two energy equations are needed and these will be chosen as the over-all energy equation

$$\rho(D/Dt)[H + (v^2/2)] + \nabla\cdot\vec{q} - \vec{E}\cdot\vec{j} = 0 \qquad (11)$$

and the electron energy equation,

$$\nabla(\rho_e h_e \vec{v}) = \vec{E}\cdot\vec{j}_e - e n_e \vec{E}\cdot\vec{v} - IR_i - \nabla\cdot\vec{q}_e$$
$$+ (n_e m_e/\tau_{ie})[3k(T_i - T_e)/m_i$$
$$+ \vec{j}\cdot\vec{j}_i/(en_e)^2 + \vec{j}\cdot\vec{v}/(en_e)] \qquad (12)$$

where

$$H = \frac{1}{\rho}[\frac{5}{2}\Sigma kn_s T_s + In_e],$$

$$\rho_e h_e = \frac{5}{2} kn_e T_e + In_e \qquad (13)$$

and $\vec{q}$ and $\vec{q}_e$ are the total and electron heat flux vectors, respectively.

The one-dimensional equations are obtained from the above equations by letting

$$\vec{v} = \vec{i}_x u_x + \vec{i}_\theta u_\theta, \quad \vec{j} = \vec{i}_x j_x + \vec{i}_r j_r + \vec{i}_\theta j_\theta,$$
$$\vec{B} = \vec{i}_x B_x + \vec{i}_r B_r, \quad \vec{E} = \vec{i}_r E_r + \vec{i}_x E_x \qquad (14)$$

Expressions for the various collision cross sections and the radiative heat loss are discussed next. The ion-electron cross section is obtained by assuming that charged particles' collisions follow Coulomb's law.

In this case, the resulting expression depends on the cut-off distance. Using Spitzer's[8] suggestion, one can write for argon,

$$Z_{ie} = 2.96\times10^{-16}\theta_e^{-2}$$
$$\times \ell n[3.441\times10^6(\theta_e^3/n_e)^{1/2}], \quad cm^2 \qquad (15)$$

where

$$\theta_s = kT_s/I \qquad (16)$$

The ion-atom collision cross section was calculated from Cramer's[9] data. The resulting expression for argon can be represented as

$$Z_{ia} = 16.383\times10^{-15}\{1 - [0.1302$$
$$-0.648\times10^{-2} \ell n(7.88\theta_i)]$$
$$\times \ell n(7.88\theta_i)\}, \quad cm^2 \qquad (17)$$

Following Petschek and Byron[10], the ionization cross section is assumed to have the representation,

$$Q(\epsilon) = a_{ea}(\epsilon - I),$$
$$a_{ea} = 4.375\times10^{-6}, \quad cm^2/erg \qquad (18)$$

The resulting expression for $f(T_e)$ is in good agreement with that obtained by Lin[11] using tabulated data in Massey and Burhop[12].

The quantities, $\nabla\cdot\vec{q}$ and $\nabla\cdot\vec{q}_e$ represent the heat loss by conduction, $\nabla\cdot\vec{q}_c$ and $\nabla\cdot\vec{q}_{ec}$ and radiation $\nabla\cdot\vec{q}_R$ and $\nabla\cdot\vec{q}_{eR}$. For an optically thin plasma, an expression for the radiation heat flux was given by Lin[11]:

$$\nabla\cdot\vec{q}_R = \nabla\cdot\vec{q}_{eR} = IR\{(\alpha/1-\alpha)L_1 + \eta L_2\} \qquad (19)$$

where, for argon

$$L_1 = 1.647\times10^{-6}(1+2\theta_e)^{-1} \exp(1/\theta_e)\{1$$
$$+ 1.0206[\theta_e^{-1} + 3 + 6\theta_e(1+\theta_e)]\}$$

$$L_2 = 0.49 \exp(0.3/\theta_e) \qquad (20)$$

and η is a number between zero and 1; the zero value corresponds to the case of a dense gas at low degree of ionization while the unity corresponds to the case of a highly rarefied gas at high degree of ionization. In the calculation reported here, η is chosen as 0.6.

In problems of discharges, it is desired to calculate the flow field, current densities and the components of the electric field for a given current (or voltage), mass flow rate and magnetic field distribution. To relate the total current to the current densities, an integrated form of the charge conservation equation,

$$\nabla\cdot\vec{j} = 0 \qquad (21)$$

will be employed. If R_a designates the radius of the anode at $x = 0$, R_c, the radius of the cathode, and $x=x_0$ denotes the tip of the cathode, then from Fig. 1 and Eq. (21), one

can write

$$A_o j_x + 2\pi R_o \int_0^x j_r dx = -J_T$$

where

$$J_T = J(x/x_o)^\ell, \quad A_o = \pi(R_o^2 - R_c^2), \quad x \leq x_o$$

$$J_T = J, \quad A_o = \pi R_o^2, \quad x \geq x_o \qquad (22)$$

where J is the total current and ℓ is some constant. Using Eqs. (9) and (14), it is seen that Eq. (22) gives a relation between E_x and E_r. Within the framework of one-dimensional theory, no additional relations between E_x and E_r can be obtained and, therefore, some assumptions must be introduced. It should be pointed out that the problem is peculiar to variable area devices and does not arise when the area is constant because $E_x=0$.

In the present analysis, different methods are employed to estimate E_x and E_r. The first assumes that either E_x or E_r is zero. The second derives an approximate relation between E_x and R_r from the consideration that both the anode and cathode are constant potential lines. Thus, since

$$dV = (\partial V/\partial x)dx + (\partial V/\partial r)dr = -E_x dx - E_r dr$$

one may write, approximately,

$$E_x = -E_r(dR/dx) \qquad (23)$$

where R designates the radius of the cathode or anode. It should be noted that Eq. (23) is not valid across the device. The third method assumes that the voltage is given; this gives an additional relationship between E_x and E_r. There is always the possibility of assuming that one of the current densities is zero. Such possibility, however, was not investigated here.

The first and second procedures result, for a given total current, in a voltage that varies with the axial distance. Also, in such cases, one cannot predict the extent of the power input region because the total power input is not given. These difficulties do not arise when both the voltage and total current are given.

It is assumed here that the plasma is magnetically contained outside the engine. The shape of the magnetic nozzle can, in principle, be calculated from the magnetic field distribution given in Ref. 3; however, the B_r measurements are not detailed enough outside the nozzle. Because of this, the shape of the magnetic nozzle is obtained from considerations similar to those given in Ref. 13. From the requirement that

$$\int \vec{B} \cdot d\vec{A}$$

through the nozzle be constant, one concludes that $B \propto 1/A$. If it is further assumed that the magnetic field is produced by a single coil of radius 'a', so that, along the axis, $B \propto [1 + (x/a)^2]^{-3/2}$; hence,

$A = A_o[1 + (x/a)^2]^{3/2}$. A_o is determined from the consideration that when $x = x_e$, $A = A_e$, where 'e' denotes exit conditions. Thus,

$$A/A_e = \{[1 + (x/a)^2]/[1 + (x_e/a)^2]\}^{3/2} \qquad (24)$$

Thus, the magnetic field distribution employed is that of Ref. 3 for B_x, and for B_r inside the nozzle. Outside the nozzle, B_r is determined from the equation

$$B_r/B_x = dR_m/dx \qquad (25)$$

where R_m is the radius of the magnetic nozzle which can be calculated from Eq. (24).

3. Results and Discussion

The calculations were carried out for argon using the geometry shown in Fig. 1. The mass flow rate and total current were chosen as 0.02 g/sec and 450 amps, respectively, ℓ in Eq. (22) was chosen as 3, and the initial pressure was assumed to be 0.33 mm of mercury.

For a given total current, magnetic field strength, and mass flow rate, one does not have enough information to calculate both E_x and E_r. The three cases discussed here were: (i) $E_r=0$, $E_x \neq 0$; (ii) $E_x=0$, $E_r \neq 0$; and (iii) $E_x = -E_r(dR/dx)$. Two sets of calculations were carried out for each of the above cases. In the first set, it was assumed that $\nabla \cdot \vec{q}_c = \nabla \cdot \vec{q}_{e,c} = 0$, M=1 occurs at the nozzle exit, and no power is added in the plume. The second set assumes that

$$\nabla \cdot \vec{q}_c = (1-\epsilon)\vec{E} \cdot \vec{j}, \quad \nabla \cdot \vec{q}_{e,c} = (1-\epsilon)\vec{E} \cdot \vec{j}_e \qquad (26)$$

where, in the subsonic region, ϵ is a given constant, and in the supersonic region, ϵ is selected in such a way so as to insure an increasing Mach number. In this case, the location of the sonic point is not known a priori, and a virtual anode is assumed so that power is added in the plume.

Typical results for case (i), i.e., $E_r=0$, $E_x \neq 0$, using the above computational schemes are shown in Figs. 2-4. The curves labelled $\epsilon = \epsilon_i = 1$ refers to the case of zero conduction losses while the curve labelled $\epsilon_i = 1$ indicates that conduction losses in the subsonic region are zero. The cut-off point in these figures corresponds to the location where T_i is about 100°C. Comparison of these results with the measurements of Ref. 3 shows that electron temperature predictions are in good agreement with experiment but the velocity is underpredicted by a factor of about 3; an electron temperature of 30,000°K to 40,000°K and a velocity of 12,000 m/sec were measured in Ref. 3. Figure 5 compares the axial velocity for cases (i) and (iii) with dR/dx based on the anode diameter. It is seen that there is a slight increase in the axial velocity when both components of the electric field are not zero. The results for case (iii) also indicate a higher rotational velocity but a lower electron tem-

4

perature. No improvement in the axial velocity was noticed when the calculations were carried out for case (ii). In all of the above calculations, the actual power supplied to the arc was of the order of 0.6 KW; this is responsible for the low axial velocities.

The other alternative to the above approach is to assume a given voltage. The measured voltage is about 45 volts. Because MPD arcs can operate in more than one voltage mode[14,15], the calculations were carried out for voltages of 45 and 20 volts. Figures 6-8 compare the axial velocity, rotational velocity, and degree of ionization for the two voltages, and Fig. 9 compares the axial velocities for various values of ϵ in the subsonic region. From these figures it is seen that the degree of ionization and axial velocity are higher for the 20-volt case and the axial velocity increases with a decrease in ϵ_i, which is the value of ϵ in the subsonic region. (Further decrease in ϵ_i results in subsonic flow throughout.) For the cases investigated, the actual power input was in the range of 0.6-1.1 KW.

The above results follow from the consideration that, for efficient heating and ionization, the flow must be subsonic. Thus the higher axial velocities and degrees of ionization are characterized by a delayed transition to supersonic velocities and more power going into the arc.

Although the delay in transition to supersonic velocities has a large influence on the axial velocity, degree of ionization, and efficiency, the rotational velocity seems to be influenced more by the value of E_r. Thus, for the case where $E_r=0$, $E_x \neq 0$, the rotational velocity was insignificant; while for the case where E_r was not zero, the rotational velocity was a large fraction of the axial velocity. In general, the rotational velocities will not behave as indicated in Fig. 7 because of the expected conversion of rotation into axial motion. If one assumes that the rotational energy is converted into axial motion, the resulting velocity is about 6000 m/sec or half the velocity measured in Ref. 3.

The calculations also indicate that the current densities have a peak in the neighborhood of the cathode tip; however, they do not exhibit any unusual behavior in the transonic region[5]. In general, the Hall current densities were less than axial and radial current densities; a result which is in agreement with Powers'[16] measurements.

For all the cases considered in this investigation, the power input up to the point where the calculations were terminated did not exceed 4 KW; this is much less than experimentally determined values. This discrepancy in the power input, which is responsible for the axial velocity being off by a factor of 2 to 3, may be a result of the following factors. The first is the neglect of second ionization; however, de-

grees of ionization calculated did not exceed 25%, and for such values the second ionization is not expected to be important. The second is that the wall losses are more than has been assumed here; this would result in higher power inputs and delayed transition to supersonic velocities. Based on the calculations carried here, the transition would have to take place outside the nozzle. In such a case, the possibility of gas entrainment exists and the effective and metered $\dot{m}$ will be different. Thus, there is a distinct possibility that the actual flow rates are higher than metered flow rates. An increased mass flow rate can partially account for the discrepancy because more power is needed to bring about transition to supersonic velocities.

4. Concluding Remarks

The results of the calculations point to the conclusion that most of the published data on MPD arcs refer to situations where transition to supersonic velocities takes place outside the engine. If this is the case, then a three-dimensional model would be needed to explain the published data. The results also suggest that improved performance can result if transition to supersonic velocities is delayed. On the other hand, to avoid any uncertainties regarding the flow rate and to reduce entrainment, the transition to supersonic velocities should take place within the nozzle. The design that meets both of these requirements is the one where the sonic velocity occurs at the exit.

References

[1]Nerheim, N. M., and Kelly, A. J., "A Critical Review of the State-of-the-art of the MPD Thrustor," AIAA Paper No. 67-688, AIAA Electric Propulsion and Plasmadynamics Conference, Colorado Springs, Colorado, Sept. 11-13, 1967.

[2]Sutton, G. W., and Sherman, A., Engineering Magnetohydrodynamics, 1st ed., McGraw-Hill, New York, 1965, pp. 111-123, 198-201.

[3]Burlock, J., Brockman, P., Hess, R. V., and Brooks, D. R., "Measurements of Velocities and Acceleration Mechanism for Coaxial Hall Accelerators," AIAA Journal, Vol. 5, No. 6, March, 1967, pp. 558-561.

[4]Shapiro, A. H., The Dynamics and Thermodynamics of Compressible Fluid Flow, 1st ed., Ronald Press, New York, 1953, Vol. 1, pp. 219-260.

[5]Workman, J. B., "Arc Structure in a Magnetic Annular Discharge," Research Report 277, June, 1967, Avco Everett Research Laboratory, Everett, Massachusetts.

[6]Hassan, H. A., Hess, R. V., and Grossmann, W., "Study of Coaxial Hall Current Accelerators at Moderate Pressure," NASA TN D-3286, October, 1966.

[7]Cowling, T. G., _Magnetohydrodynamics_, 1st ed., Interscience, New York, 1957, pp. 105-107.

[8]Spitzer, L., Jr., _Physics of Fully Ionized Gases_, 2nd ed., Interscience, New York, 1962, p. 127.

[9]Cramer, W. H., "Elastic and Inelastic Scattering of Low-velocity Ions: Ne^+ in A, A^+ in Ne, A^+ in A," _The Journal of Chemical Physics_, Vol. 30, No. 3, March, 1959, pp. 641-642.

[10]Petschek, H., and Bryon, S., "Approach to Equilibrium Ionization Behind Strong Shock Waves in Argon," _Annals of Physics_, Vol. 1, No. 3, June, 1957, pp. 270-315.

[11]Lin, S. C., "Limiting Velocity for a Rotating Plasma," _The Physics of Fluids_, Vol. 4, No. 10, October, 1961, pp. 1277-1288.

[12]Massey, H. S. W., and Burhop, E. H. S., _Electronic and Ionic Impact Phenomena_, 1st ed., The Clarendon Press, Oxford, 1952.

[13]John, R. R., and Bennett, S., "Arcjet Technology Research and Development," RAD-TR-65-37, December, 1965, Research and Advanced Development Division, Avco Corporation, Wilmington, Massachusetts.

[14]Bennett, S., Enos, G., John, R., and Powers, W., "Development of an Ammonia-fueled MPD Arc Jet Thrustor," AIAA Paper No. 67-690, AIAA Electric Propulsion and Plasmadynamics Conference, Colorado Springs, Colorado, Sept. 11-13, 1967.

[15]Connolly, D. J., Sovie, R. J., Michels, C. J., and Burkhart, J. A., "Low Environmental Pressure MPD Arc Tests," AIAA Paper No. 67-685, AIAA Electric Propulsion and Plasmadynamics Conference, Colorado Springs, Colorado, Sept. 11-13, 1967.

[16]Powers, W. E., "Measurements of the Current Density Distribution in the Exhaust of an MPD Arcjet," _AIAA Journal_, Vol. 5, No. 3, March, 1967, pp. 545-550.
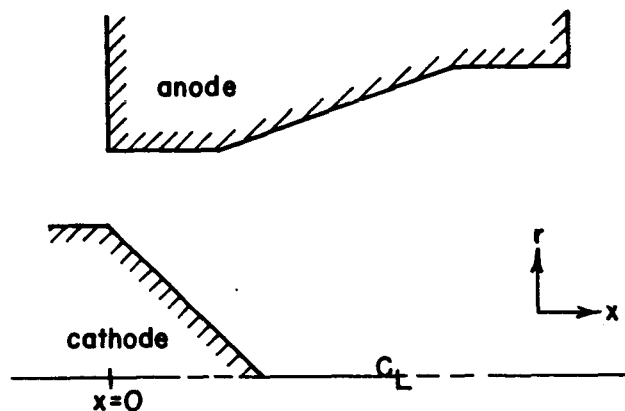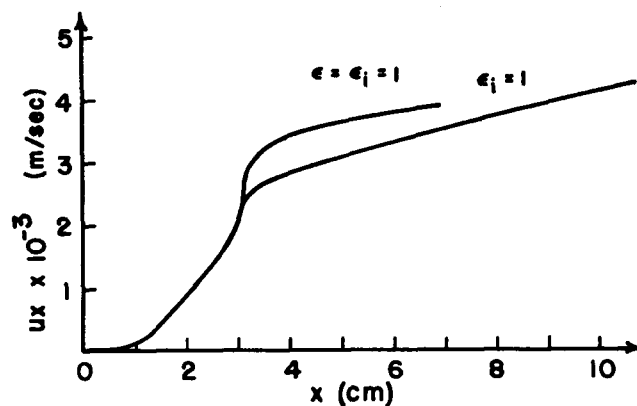
Figure 1. Schematic of MPD Arc

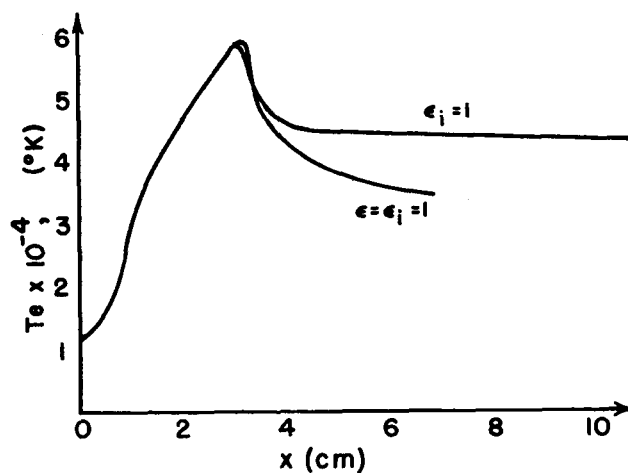Figure 2. Axial Velocity vs. Distance ($E_r=0$, $E_x \neq 0$)

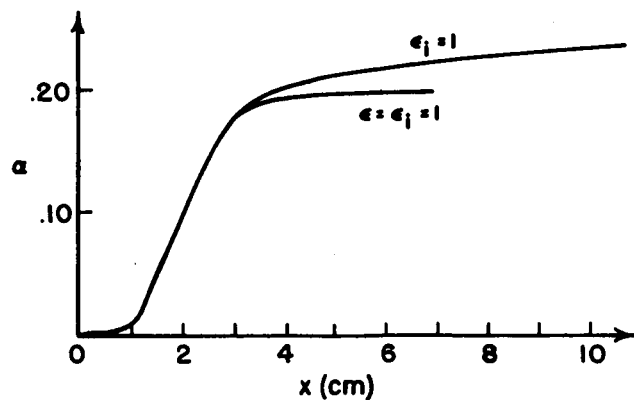Figure 3. Electron Temperature vs. Distance ($E_r=0$, $E_x \neq 0$)

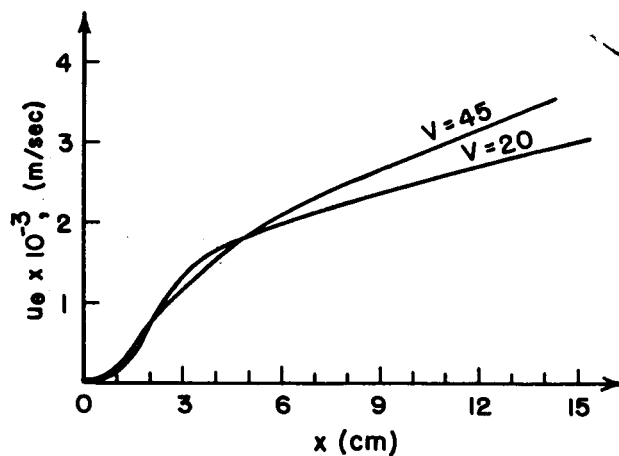Figure 4. Degree of Ionization vs.
Distance ($E_r=0$, $E_x \neq 0$)

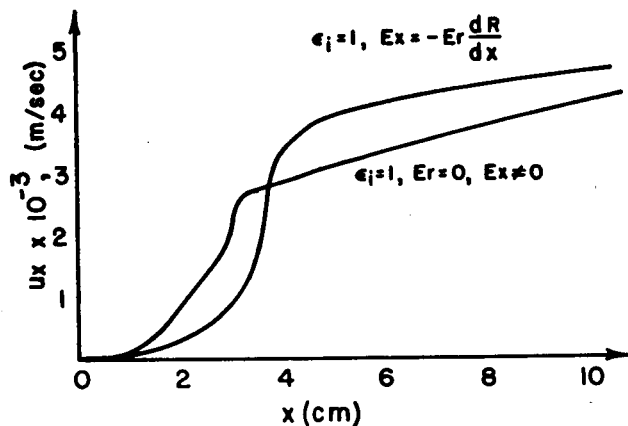Figure 7. Rotational Velocity vs. Distance
($\epsilon_i = .8$)

Figure 5. Axial Velocity vs. Distance

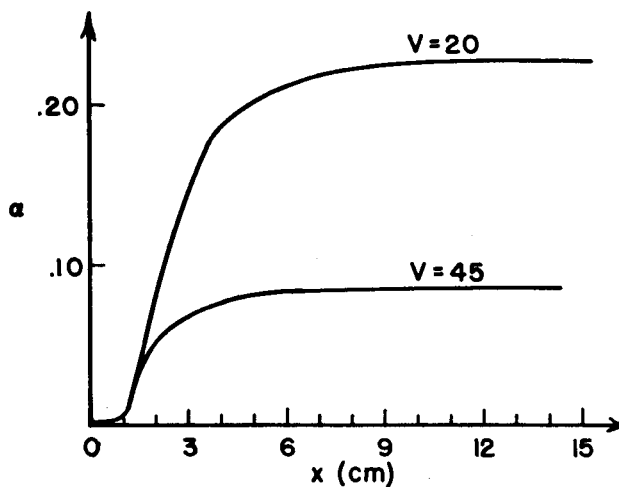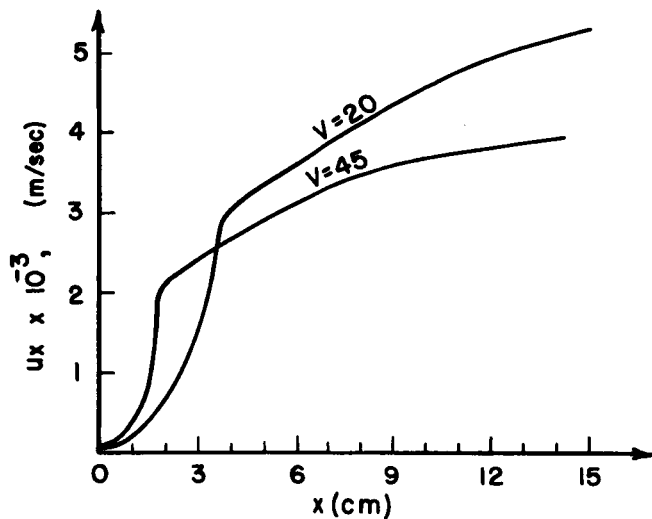Figure 8. Degree of Ionization vs.
Distance ($\epsilon_i = .8$)
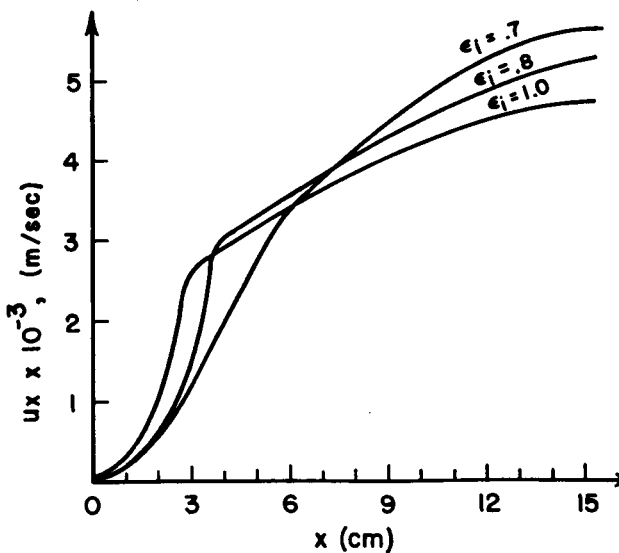
Figure 6. Axial Velocity vs. Distance
($\epsilon_i = .8$)

Figure 9. Axial Velocity vs. Distance
(V = 20 volts)

7